INSTITUTE OF PHYSICS PUBLISHING JOURNAL OF OPTICS A: PURE AND APPLIED OPTICS

J. Opt. A: Pure Appl. Opt. **7** (2005) 324–332 doi:10.1088/1464-4258/7/7/010

Spontaneous grating formation in thin light-sensitive AgCl–Ag films at linear P/S-polarization of a laser beam

E D Makovetsky, V K Miloslavsky and L A Ageev

Department of Physics, Kharkov VN Karazin National University,
4 Svobody Square, 61077 Kharkov, Ukraine

E-mail: evgeny.d.makovetsky@univer.kharkov.ua

Received 29 December 2004, accepted for publication 4 April 2005
Published 21 June 2005
Online at stacks.iop.org/JOptA/7/324

Abstract

We investigated the development of spontaneous gratings arising in light-sensitive waveguide AgCl–Ag films on glass substrates at various cases of linear polarization of the single inducing laser beam. The cause of such a grating development is the appearance of an interference field created by the summation of the incident beam and scattered waveguide TE- and TM-modes. Positive feedback in grating growth is provided by Wood's anomalies taking place for all the gratings, and the simultaneous development of many microgratings results in their competition. Earlier we found that two-dimensional Bragg's diffraction seriously affects this competition. This kind of diffraction results in the appearance of secondary dominant gratings. Now we found that at the beam's polarization, deviated from P-polarization, the appearance of tertiary gratings becomes possible due to the Bragg's diffraction on secondary dominant gratings instead of this diffraction on primary gratings. The influence of the existence of the first and second steps in two-dimensional diffraction on grating growth is proved by both optical microscopy and complete identification of the modes excited in the substrate and in air (radiative modes in small-angle scattering pattern).

Keywords: spontaneous gratings, thin light-sensitive films, waveguide modes, Wood's anomalies, Bragg's diffraction, small-angle scattering

1. Introduction

There are a number of photosensitive materials in which photoconversions are carried out in real time. These are amorphous chalcogenide semiconductors [1], photopolymers [2, 3], etc. These materials are used in the optical holography technique, particularly in recording holographic gratings with high spatial frequencies [4, 5]. For the mentioned purposes these materials are usually used in the form of a thin film. Irradiation of the film may be conducted either at the spectral region of high absorption (the absorption index is $\kappa = 0.1$–1) or at the relatively transparent region ($\kappa < 0.1$). In the latter case the thin films evince their waveguide properties when deposited on a substrate with a refraction index lower than that of the film. An inevitable scattering of light in the photolayer may excite waveguide TE- and TM-modes. Interference of incident beam and scattered modes promotes the formation of spontaneous (noisy) gratings [6]. The existence of noisy gratings may significantly reduce the quality of holographic gratings written by the two beams. For example, in polymer waveguides used in [3] about 30% of the power of light diffracted on all photoinduced gratings is wasted on the 'satellite' beams appearing due to noisy gratings. So in the process of hologram creation spontaneous gratings (SGs) are undesirable. Investigations of SGs at a two-beam scheme were also carried out by our research group (see [7]). On the other hand, SGs arise at single laser beam action, and their appearance is interesting as a nonlinear optical effect.

The SGs in photolayers are in many aspects similar to the gratings formed on metal or semiconductor surfaces under the action of a strong laser beam [8, 9]. However, SGs of these two types differ essentially in their formation

mechanism and structure of directed modes on which SGs are formed. While SGs on solid surfaces grow on scattered surface TM-modes and form a periodical surface relief, the SGs in photolayers are developed on scattered waveguide TE- and TM-modes, and the grating appearance is associated with the film's dielectric permittivity modulation. The number of TE_m- and TM_m-modes and their propagation constants depend on the photolayer thickness. The cut-off thicknesses of the modes are also different. All of this results in a greater diversity of SGs in photolayers (see review [6]) in comparison with periodical structures on solid surfaces (see review [8]). When both the film thickness and angle of incidence are small, SGs are developed on scattered TE-modes. However, at $h \geqslant h_{TM_0}$ (h_{TM_0} is the cut-off thickness of the TM_0-mode) and at large angle of incidence, SGs are formed on TM-modes. An intermediate case is possible when SG formation occurs at strong competition of TE_m- and TM_m-modes, and this problem is almost uninvestigated. There are a small number of works on this question [3, 10–12].

In this paper we present the results of the investigation of SG appearance and growth in light-sensitive AgCl films containing granular silver. Photoconversions in these films are carried out in real time. Thin AgCl films are almost insensitive to weak laser radiation in the visible frequency range. When brought into the film, granular silver creates a colloidal absorption band. This band is centred at 500 nm and covers almost all the visible range. Irradiating the film by a monochromatic beam leads to hole-burning in the absorption band, i.e. to an increase of film transparency at the wavelength of irradiation, and to the excitation of waveguide modes [13]. Transfer of Ag granules from maxima to minima of the interference field (appearing at incident wave interaction with a mode) leads to the formation of SGs. Both diffraction efficiency and orientation of grooves of various SGs depend on indicatrices of radiation scattered in TE- and TM-modes. The indicatrices, in their turn, depend on the polarization and angle of incidence of the beam. We investigated the development of SGs at the mentioned conditions of competition of only two modes—TE_0- and TM_0-modes. Therefore, below, to shorten the designations of SG grating vectors and modes, we will write 'TE-' and 'TM-' meaning 'TE_0-' and 'TM_0-'. When investigating the SG formation at linear P-polarization and at mixed P/S-polarization, we found a principal change in the process of SG development at a comparatively small portion of S-component in the incident beam. Though there are a number of peculiarities in the diffraction patterns and their time evolution, we have explained all of the peculiarities using the model of two-dimensional Bragg diffraction.

2. General background

The SGs appear at interference of incident wave and modes excited due to light scattering in the film, so the vector of a planar SG depends on the angle of incidence φ and azimuth α of the scattered mode:

$$\boldsymbol{K} = (\beta\cos\alpha - k_x)\boldsymbol{i} + \beta\sin\alpha\boldsymbol{j} \qquad (1)$$

where $\boldsymbol{i}$ and $\boldsymbol{j}$ are the unit vectors of axes x and y in the layer plane, axis x lies at the intersection of the incidence plane and the sample plane, $\boldsymbol{\beta}$ is a vector of the waveguide mode, $\alpha = \angle(\boldsymbol{\beta}, \boldsymbol{i})$, $k_x = k_0\sin\varphi$, $k_0 = 2\pi/\lambda$. The planar character of the SGs is defined by the small thickness of the waveguide layer and is confirmed experimentally by measurements of the grating period $d = 2\pi/K$. The SG having appeared, diffraction of the incident beam on the SG takes place. The tangential component of the diffracted wave is

$$\boldsymbol{k}_d = \boldsymbol{k}_x + m\boldsymbol{K} = [k_x + m(\beta\cos\alpha - k_x)]\boldsymbol{i} + m\beta\sin\alpha\boldsymbol{j}, \quad (2)$$

where $m = \pm1, \pm2, \ldots$ is a diffraction order, and the grating vector $\boldsymbol{K}$ is substituted from (1). It follows from (2) that $\boldsymbol{k}_d = \boldsymbol{\beta}$ at $m = 1$, i.e. the SG automatically enters the same mode on which it grows (Wood's anomaly), so the SG develops due to positive feedback. But for $m = -1$ we get $k_{dx} = 2k_x - \beta\cos\alpha$, i.e. $\boldsymbol{k}_d \neq \boldsymbol{\beta}$ in the general case. The wave diffracted at $m = -1$ appears as a leaky mode if $k_d < n_s k_0$ or as mode damped in the photolayer if $k_d > n_s k_0$, where n_s is the substrate refractive index. But there are exceptions: some azimuths α for which diffraction at $m = -1$ order also excites waveguide modes.

It is useful to distinguish the cases of single-mode and two-mode films. In the former case at azimuth α^* (governed by the condition $\beta\cos\alpha^* = k_x$) an SG with $\boldsymbol{K} = \sqrt{\beta^2 - k_x^2}\boldsymbol{j}$ arises. Diffraction on it at $m = -1$ results in the excitation of a mode with vector $\boldsymbol{\beta} = k_x\boldsymbol{i} - \sqrt{\beta^2 - k_x^2}\boldsymbol{j}$ on which the grating with $\boldsymbol{K}' = -\sqrt{\beta^2 - k_x^2}\boldsymbol{j}$ grows. In contrast, diffraction at $m = -1$ on this SG enters the mode on which the initial grating with $\boldsymbol{K} = \sqrt{\beta^2 - k_x^2}\boldsymbol{j}$ grows. So these two SGs intensify each other's growth. These gratings are so-called [14] degenerated C-gratings growing at double Wood's anomaly. Their vectors are antiparallel, and the diffraction efficiency exceeds the efficiency of SGs growing at ordinary Wood's anomalies [8]. C-gratings were discovered at irradiation of solid surfaces by a powerful laser beam [9, 14, 15].

Let β_1 and β_2 be vectors of two different modes propagating in the film. They may be of the same type (in all possible cases) or of different types (in a two-mode case mentioned above, and in more complicated cases).

Suppose that an SG grows on a mode with vector $\boldsymbol{\beta}_1$ propagating at azimuth α_1. Let diffraction into $m = -1$ order on this SG enter a mode with vector β_2 under azimuth α_2. Equating the components of the second mode to the components of the wave diffracted at $m = -1$ on the first SG, we have

$$\beta_1\cos\alpha_1 = k_x - \frac{\Delta}{4k_x}, \qquad \beta_1\sin\alpha_1 = -\beta_2\sin\alpha_2, \quad (3)$$

where $\Delta = \beta_2^2 - \beta_1^2$. The conditions (3) are implicit definitions of α_1 and α_2 as functions of β_1, β_2, k_x.

In the case of a single-mode film $\beta_1 = \beta_2 = \beta_{TE}$. Therefore both α_1 and α_2 have only one possible value each, and there is only one pair of C-gratings. They have vectors $\boldsymbol{K}_C = \pm\sqrt{\beta_{TE}^2 - k_x^2}\boldsymbol{j}$ and amplify each other at beam diffraction into -1 order.

In the case of a two-mode film each of β_1 and β_2 may be assumed to be β_{TM} or β_{TE} ($\beta_{TE} > \beta_{TM}$), so there are four variants of α_1 and α_2, i.e. four pairs of C-gratings. In each pair SGs have antiparallel vectors and equal periods, and grow at double Wood's anomalies as ordinary C-gratings grow in the single-mode case.

Thus, in contrast to the single-mode case for which only two C-gratings grow at $\varphi \neq 0°$, in the two-mode case simultaneous growth of eight C-gratings is possible though scattering indicatrices for linear polarization do not allow simultaneous growth of all of them. Two pairs of C-gratings grow on modes of the same type scattered under such α_1, α_2 that $\beta_1 \cos\alpha_1 = \beta_2 \cos\alpha_2 = k_x$. Their vectors are

$$\boldsymbol{K}_{1,2} = \pm\sqrt{\beta_{\mathrm{TM}}^2 - k_x^2}\,\boldsymbol{j}, \qquad \boldsymbol{K}_{3,4} = \pm\sqrt{\beta_{\mathrm{TE}}^2 - k_x^2}\,\boldsymbol{j}. \quad (4)$$

Four new SGs grow on the modes scattered under α_1, α_2 subjected to conditions (3) at $\beta_1 \neq \beta_2$. They have vectors

$$\begin{aligned} \boldsymbol{K}_{5,6} &= -\frac{\Delta}{4k_x}\boldsymbol{i} \pm \sqrt{\beta_{\mathrm{TM}}^2 - \beta_{\mathrm{TM},x}^2}\,\boldsymbol{j}, \\ \boldsymbol{K}_{7,8} &= \frac{\Delta}{4k_x}\boldsymbol{i} \pm \sqrt{\beta_{\mathrm{TE}}^2 - \beta_{\mathrm{TE},x}^2}\,\boldsymbol{j}. \end{aligned} \quad (5)$$

Here $\Delta = \beta_{\mathrm{TE}}^2 - \beta_{\mathrm{TM}}^2$. The gratings with vectors (5) were found out in [10] at a circularly polarized beam acting through a prism. A continuous spectrum (caused by β value spread) of C-gratings on scattered modes with azimuths near α^* was found in [12].

The SG growth depends on indicatrices of light scattered in the film. The shape of the indicatrix depends on the size and density of the scattering centres, and on beam polarization. The simplest case is the one of a spherical scattering centre with radius $a \ll \lambda$. This case is typical for Ag granules in AgCl film [6]. It is also assumed that a small concentration of granules takes place. If so, then there is only one-fold scattering. Calculations with the help of an amplitude matrix of scattering [16] show that at an S-polarized beam the intensities of radiation scattered to waveguide TE- and TM-modes are

$$I_{\mathrm{S,TE}} \propto \cos^2\alpha, \qquad I_{\mathrm{S,TM}} \propto \sin^2\alpha\cos^2\theta, \quad (6)$$

where $\theta = \angle(\boldsymbol{k}_{\mathrm{s}}, z)$ is a meridional angle, $\boldsymbol{k}_{\mathrm{s}}$ is the wavevector of the scattered wave, z is a normal to the film. At P-polarization of the laser beam the intensities are

$$\begin{aligned} I_{\mathrm{P,TE}} &\propto \sin^2\alpha\cos^2\psi, \\ I_{\mathrm{P,TM}} &\propto (\cos\alpha\cos\theta\cos\psi + \sin\theta\sin\psi)^2, \end{aligned} \quad (7)$$

where ψ is the angle of the refracted incident wave. It follows from (6) and (7) that I_{TM} depends on β_{TM}, for in the ray approximation [17] $\beta_{\mathrm{TM}} = k_0 n\sin\theta$, where n is the film's index of refraction. Besides, at P-polarization $I_{\mathrm{P,TE}}$ and $I_{\mathrm{P,TM}}$ depend on φ because $n\sin\psi = n_0\sin\varphi$. At φ increase $I_{\mathrm{P,TM}}$ may exceed $I_{\mathrm{P,TE}}$. At a mixed P/S-polarization the intensities of the scattered light depend on the angle χ between the planes of polarization and incidence. $I_{\mathrm{PS,TE}}$ and $I_{\mathrm{PS,TM}}$ may be found by summation of the electric fields of radiation scattered at S- and P-polarization. Also we must consider amplitudes τ_{S} and τ_{P} of the waves passed through the photolayer–outer medium boundary at corresponding polarizations. If $\varkappa = \tau_{\mathrm{P}}/\tau_{\mathrm{S}}$, then

$$\begin{aligned} I_{\mathrm{PS,TE}} &\propto (-\cos\alpha\sin\chi + \varkappa\sin\alpha\cos\psi\cos\chi)^2, \\ I_{\mathrm{PS,TM}} &\propto [\sin\alpha\cos\theta\sin\chi \\ &\quad + \varkappa(\cos\alpha\cos\theta\cos\psi + \sin\theta\sin\psi)\cos\chi]^2. \end{aligned} \quad (8)$$

The dependences (8) define the scattering indicatrices at scattering into the front hemisphere. True indicatrices are obtained when we add analogous scattering into the rear hemisphere (they are the same indicatrices turned by 180°).

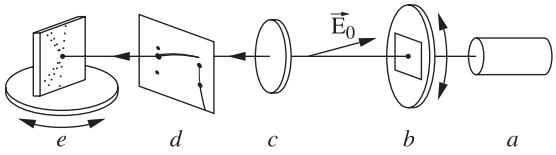

Figure 1. Experimental setup for the creation of spontaneous gratings and observations of small-angle scattering patterns. Here *a*—a He–Ne laser, *b*—a quartz $\lambda/2$-plate on a vertical goniometer, *c*—a converging lens, *d*—a screen with schematic image of the small-angle scattering (SAS) pattern (see figure 2), *e*—the AgCl–Ag film on a horizontal goniometer (resolution 5′), and schematic rows of light spots on the sample (see figure 3(a)).

3. Experiment

The experiment was carried out on AgCl–Ag films prepared by deposition of substances onto a plane-parallel glass substrate in vacuum ($n_{\mathrm{s}} = 1.515$, thickness $H = 1.8$ mm). The film thickness $h = 100$ nm was taken between cut-off thicknesses $h_{\mathrm{TM}_0} = 94$ nm and $h_{\mathrm{TE}_1} = 273$ nm of corresponding waveguide modes. The specific volume of silver in the AgCl–Ag film was 0.1. The sample was irradiated by a linearly polarized Gauss beam of a He–Ne laser (single-mode generation, $\lambda = 632.8$ nm, output power $P = 8$ mW, waist spot radius $w_0 = 3 \times 10^{-2}$ cm at the output mirror). The irradiation scheme is presented at figure 1.

The beam passed through a quartz $\lambda/2$-plate installed on a vertical goniometer. This plate was used to rotate the polarization plane of the beam. Then the beam was focused on the sample (installed on a horizontal goniometer) by a lens with $F = 8.5$ cm. Between the lens and sample there was a screen with a hole for the beam transmittance. The screen is needed to observe diffraction patterns appearing at SG development. The irradiated region on the sample had an elliptic form and area $S_{\mathrm{F}}(\varphi) = S_{\mathrm{F}}(0)\sec\varphi$. The focal area $S_{\mathrm{F}}(0) \approx 2000\ \mu\mathrm{m}^2$ was calculated by formulae for a Gauss beam [18]. The incident angle $\varphi = 49°40'$ was chosen because of the following. First, it follows from (7) that, at this angle, P-polarization and film's refractive index $n = 2.06$, the ratio

$$\rho = \frac{I_{\mathrm{P,TM,max}}}{I_{\mathrm{P,TE,max}}} = \frac{I_{\mathrm{P,TM}}(\alpha = 0)}{I_{\mathrm{P,TE}}(\alpha = \pi/2)} \quad (9)$$

is near 1. This provides competition of TE- and TM-modes at SG development. The ratio (9) is increased also at film thickness close to cut-off thickness h_{TM_0}. Second, at this angle of incidence the condition $\beta_{\mathrm{TM}_0} = 2k_x$ is met. Thus diffraction to $m = -2$ order from an S$_-$-SG (formed at $\alpha = 0$, $\boldsymbol{K}_{\mathrm{S}_-} = (\beta_{\mathrm{TM}_0} - k_x)\boldsymbol{i}$) results in a beam directed to meet the original beam. This provides an easy control of the SG development and gives a precise value of effective refractive index of TM$_0$-mode ($n_{\mathrm{TM}_0} = 2\sin\varphi$).

We took photographs of diffraction patterns at various beam polarization azimuths χ and duration of irradiation to demonstrate the evolution of the patterns. Besides, at P/S-polarization we observed a number of diffraction reflexes penetrating into the substrate provided the condition $k_0 < k_{\mathrm{d}} < n_{\mathrm{s}}k_0$ is met for the tangential component. These beams propagate in the glass–film sample, totally reflecting at boundaries with air. The beams become apparent as rows of equidistant light spots on the film. Also, we observed the

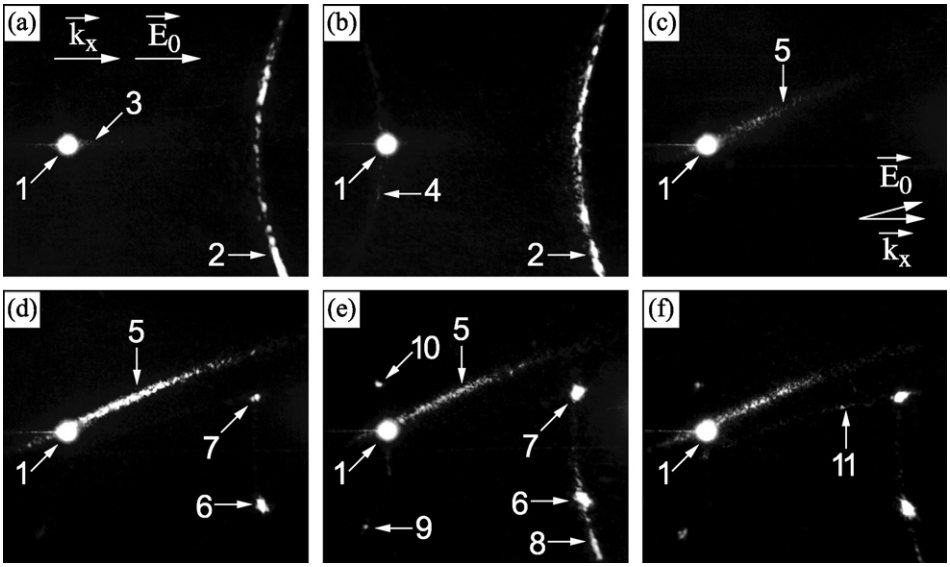

Figure 2. Photographs of small-angle scattering patterns on the screen. At angle $\chi = 0°$ between $\boldsymbol{E}_0$ and $\boldsymbol{k}_x$: (a) $t = 1$ min, (b) $t = 8$ min. At $\chi = 15°$: (c) $t = 5$ s, (d) $t = 1$ min, (e) $t = 2.5$ min. At $\chi = 20°$: (f) $t = 5$ min. Here the laser beam is marked as 1. Arcs 2, 4 and 8 are due to beam diffraction on the many S$_-$-like gratings. Scattering 3 and arcs 5, 11 are because of diffraction of waveguide modes on gratings. Spots 6, 9 and 7, 10 appear due to the existence of strong S$'_1$- and S$''_1$-gratings among weaker S$_-$-like gratings.

irradiated regions under an optical microscope to clarify the spatial distribution of various SGs.

4. Experimental results

A set of photographs of diffraction patterns on the screen at $\chi = 0°$, 15°, and 20° is presented in figure 2. On all the photographs the laser beam is marked as 1. The simplest patterns are the patterns observed at P-polarization ($\chi = 0°$, figures 2(a), (b)). The intensive vertical arc 2 (appearing after about 1 s of laser beam action) exists due to diffraction in $m = -1$ order from the so-called [14] S$_-$-like TM-gratings growing on scattered modes with azimuths close to 0°. Existence of the arc is evidence of azimuthal spread of vectors $\boldsymbol{K}$ of S$_-$-SGs which create the whole quasiperiodic structure. The arc's ends correspond to TM-mode azimuthal spread of about $\alpha = \pm 15°$ from the plane of incidence. As follows from (7), such a deviation of mode azimuth slightly changes $I_{\mathrm{P,TM}}$. So the interference field favours growth of S$_-$-SGs. The diffraction reflex (arc 2) consists of separate spots. It indicates a relatively small number of S$_-$-microgratings arising in the irradiated region under the action of a focused laser beam. Besides, a weak anisotropic scattering 3 is observed in the photograph. This converges along $\boldsymbol{k}_x$ to the centre of the laser beam. This scattering is associated with diffraction of scattered TE-modes on the so-called parquet gratings (P-gratings) growing on TE-modes at $\alpha = \pm\pi/2$ [19]. With increasing exposure, this scattering weakens (figure 2(b)), with the simultaneous appearance of the vertical arc 4 passing through the laser beam. This arc appearance is associated with laser beam diffraction into $m = -2$ order on the S$_-$-like SGs. Diffraction from them becomes possible for non-sinusoidality of the SG profile. This non-sinusoidality is acquired with exposition.

The diffraction pattern essentially changes at $\chi = 15°$ and 20° (figures 2(c)–(f)). At time t of about 1 s the horizontal arc 5 (convex upwards) appears on the screen while the reflex from S$_{-,\mathrm{TM}}$-SG in the centre of arc 2 is absent. Arc 5 appears because of the formation of the C-grating on TE-modes due to the favourable scattering indicatrix at $\chi = 15°$. With increasing exposition, arc 5 flashes and dot-like reflex 6 appear ($t = 30$ s). Then a dot-like reflex 7 appears (figure 2(d), $t = 1$ min), and in a while it becomes brighter than reflex 6 (figure 2(e), $t = 2.5$ min). At large t, arc 8 from S$_-$-like gratings (analogous to arc 2 in figures 2(a), (b)) appears. It passes through dot-like reflexes 6 and 7. Then spots 9 and 10 also become visible. Spots 6 and 9 correspond to diffraction into -1 and -2 order from one regular S$_-$-like SG on the TM-mode, and spots 7 and 10 correspond to the same diffraction on another regular S$_-$-like SG on the TM-mode. However, arc 8 from S$_-$-like gratings, unlike arc 2 at $\chi = 0°$, is asymmetrical to the plane of incidence. With further exposition the diffraction pattern becomes saturated and does not undergo any qualitative changes. At $\chi = 20°$ (figure 2(f)) the pattern is similar to the one at $\chi = 15°$, except for the appearance of new arc 11. This arc is parallel (i.e. has the same centre of curvature) to arc 5 and has reflex 7 on its end. At negative χ the pattern is reflection symmetric to the pattern at $|\chi|$.

In contrast to P-polarization, at $\chi = 15°$ a number of diffraction reflexes appear on the sample itself. The reflexes are equidistant and situated on straight lines originating from the centre of the irradiated region at various angles to the plane of incidence (figure 3(a)). These reflexes are fixed in the photolayer. They are associated with diffraction beams ($m = -1$) from new regular SGs for which $k_0 < k_{\mathrm{d}} < n_{\mathrm{s}}k_0$ or with diffraction of waveguide modes on SGs. Some reflexes have another origin. Regular diffraction gratings with comparatively large periods $d > \lambda$ were also observed under an optical microscope in reflected light. In particular, these are S$_-$-like gratings with periods close to the largest one: $d_{\mathrm{S}_-} = 830$ nm for $\varphi = 49°40'$ (see (1)). The C-gratings (with periods less than 450 nm) are not visible under an optical microscope. In figures 3(b) and (c) the regular gratings,

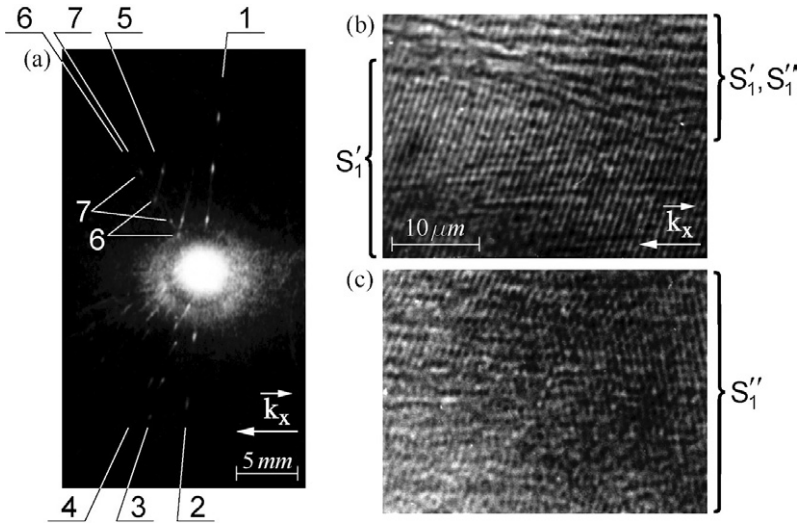

Figure 3. Photographs of irradiated AgCl–Ag film. (a) General photograph demonstrating rows of light spots starting at the irradiated region (centre of the large white spot). We determined the corresponding substrate modes by measurements of distances between spots in a row and rows' angles with the incidence plane. (b) and (c) Microphotographs of the irradiated region (obtained with an optical microscope). Secondary dominant S_1'- and S_1''-gratings are clearly visible due to their large periods, and their intersection creates pulsations.

responsible for dot-like reflexes at $\chi = 15°$, are clearly visible on the screen. In some places these gratings overlie, creating a complicated grid.

5. Discussion

Now consider the interaction of gratings developing in the film. It is grating interaction and competition that results in the development of secondary (and then tertiary) gratings which are discussed below. And it is grating interaction that creates the so-called small-angle scattering pattern (SAS pattern [20, 21]) which is the most convenient way to trace changes in light-sensitive films in real time during irradiation. The SAS pattern is formed by spots corresponding to radiative modes created by diffraction on an SG of either the incident beam or waveguide mode. Beam diffraction is described by (2). Let us consider the mode diffraction.

The azimuthal distribution (8) of light scattering in TE- or TM-modes leads to the appearance of dominant gratings corresponding to maxima of scattering to TE- or TM-modes. For example, at $\chi = 0$ among such SGs there are S$_-$-gratings (mode azimuth is $\alpha = 0$) on TM-modes and P-gratings (mode azimuth is $\alpha = \pm\pi/2$) on TE-modes. A dominant mode, excited by a dominant grating with $\boldsymbol{K}_0$, propagates in the film and diffracts on an adjacent SG with $\boldsymbol{K} \neq \boldsymbol{K}_0$. This results in the appearance of a wave with the following tangential component of wavevector:

$$\boldsymbol{k}_\mathrm{r} = \boldsymbol{\beta}_0 + m\boldsymbol{K} = [\beta_0 \cos\alpha_0 + m(\beta\cos\alpha - k_x)]\boldsymbol{i} + (\beta_0 \sin\alpha_0 + m\beta\sin\alpha)\boldsymbol{j} \quad (10)$$

where β_0 is the wavevector of the dominant mode, $m = \pm 1$. On the other hand, a mode, scattered under the azimuth α, may diffract on the dominant grating and produce a radiative mode with

$$\boldsymbol{k}_\mathrm{r} = \boldsymbol{\beta} + m\boldsymbol{K}_0 = [\beta\cos\alpha + m(\beta_0\cos\alpha_0 - k_x)]\boldsymbol{i} + (\beta\sin\alpha + m\beta_0\sin\alpha_0)\boldsymbol{j}. \quad (11)$$

One can see from (10) and (11) that these two cases produce the same result at $m = 1$ but different results at $m = -1$. When S$_-$-gratings are the dominant ones, diffraction of their modes on adjacent S$_-$-like gratings at $m = -1$ (α close to 0) results in small-angle scattering, i.e. scattering along directions with small angle to the laser beam ($\boldsymbol{k}_\mathrm{r} = \boldsymbol{k}_x$ at $\alpha = \alpha_0$). Diffraction from P-gratings ($\alpha_0 = \pm\pi/2$) is observed on the screen at $m = 1$ and α close to $\mp\pi/2$ ($\boldsymbol{k}_\mathrm{r} = -\boldsymbol{k}_x$ at $\alpha = \mp\pi/2$, figure 2(a), object 3).

An SG may become dominant not only due to a favourable scattering indicatrix. For example, C-gratings are dominant due to double Wood's anomalies which amplify their growth. Diffraction from C-gratings will be observed on the screen (arc 5 in figures 2(c)–(f)) either at $\alpha \approx \pi + \alpha_0$ and $m = 1$ (see (10)) or at $\alpha \approx \pi - \alpha_0$ and $m = -1$ (see (11)) depending on the case of diffraction. Considering the indicatrix (8) of scattered radiation at $\chi = 15°$ and more, we conclude that at such χ the upcast C-grating (see figure 4) must grow on the TM-mode while the downcast C-grating must grow on the TE-mode. These are TM-SGs with vectors $\boldsymbol{K}_1$, $\boldsymbol{K}_5$ and TE-SGs with vectors $\boldsymbol{K}_4$, $\boldsymbol{K}_8$. Among them only SGs with $\boldsymbol{K}_5$ and $\boldsymbol{K}_8$ form a pair of SGs which amplify each other's growth at beam diffraction at order $m = -1$. So these SGs must grow more intensively than the rest of the C-gratings. Indeed, there is only one arc passing through the laser beam (arc 5) in figures 2(c)–(f), so there is only one dominant downcast C-grating. The arc symmetrical to arc 5 in the lower half of the screen is absent because of weakness of corresponding waveguide modes, so we can say nothing about the number of dominant SGs among $\boldsymbol{K}_1$, $\boldsymbol{K}_3$, $\boldsymbol{K}_5$ and $\boldsymbol{K}_7$.

Formulae (10) and (11) may be extended for the two-mode case: diffraction of the mode with β_1 on an SG growing on the mode with $\beta_2 \neq \beta_1$. Such a diffraction is presented in figure 2(f). As $\beta_{\mathrm{TE}_0} > \beta_{\mathrm{TM}_0}$, arcs 5 and 11 are results of diffraction, correspondingly, of TE-modes and TM-modes on the C-grating at $m = 1$. It is arc 5 that passes through laser beam 1, so the downcast C-grating must be formed on the TE-

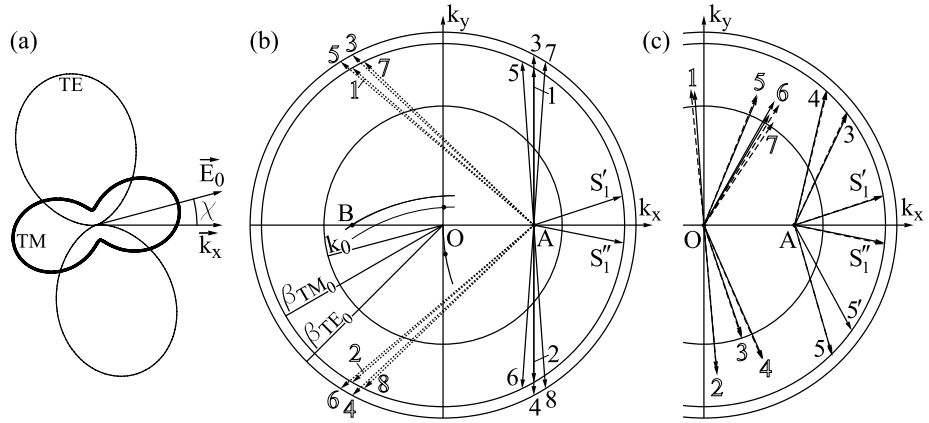

Figure 4. Indicatrices of scattering in the film, and Ewald's diagrams. (a) Scattering indicatrices for TE- and TM-modes at our film. They were calculated from (8) at $\chi = 15°$ and $\varkappa = 1.15$ as the sum of scattering into front and rear hemispheres. (b) Ewald's diagram illustrating vectors (4), (5) of all possible C-gratings (eight solid vectors with solid numbers), vectors (16), (17) of all possible C/B-gratings (eight dotted vectors with contoured numbers) and secondary S_1'- and S_1''-grating. Also shown are the arcs and spots which are visible on the screen. Point $B(-k_x, 0)$ corresponds to the incident laser beam. (c) Comparison of experimental (dashed) and calculated (solid) vectors of substrate modes 1–7 (contoured numbers; the exact values are in table 1). Also shown are the vectors of the tertiary gratings (solid numbers) including grating 5′ which creates a radiative mode which leaves the film at a sliding angle.

modes, i.e. its vector is either $\boldsymbol{K}_4$ or $\boldsymbol{K}_8$. This is in agreement with the scattering indicatrix.

To explain the appearance of dot-like reflexes on the screen and rows of light spots on the sample, we used the model of so-called two-dimensional Bragg diffraction (TBD) [22, 23]. The result of TBD is the formation of secondary gratings on waveguide modes which were amplified by such a diffraction. The formation of such structures on TM-modes was discovered earlier at the incidence of the laser beam on the photolayer through a prism [6]. The general formula describing TBD is

$$\boldsymbol{\beta}_2 = \boldsymbol{\beta}_1 + m\boldsymbol{K}_0 \tag{12}$$

where $m = \pm 1$, $\boldsymbol{\beta}_1$ and $\boldsymbol{\beta}_2$ are vectors of the modes being diffracted. Actually, formula (12) is a special case of (11) at $\boldsymbol{k}_r = \boldsymbol{\beta}_2$. If diffraction of the mode $\boldsymbol{\beta}_1$ on the grating with $\boldsymbol{K}_0$ excites a mode $\boldsymbol{\beta}_2$, then, vice versa, the mode $\boldsymbol{\beta}_2$ excites a mode $\boldsymbol{\beta}_1$. Thus two gratings (formed on interference of these modes with incident light) amplify each other's growth provided there is a dominant grating with $\boldsymbol{K}_0$.

In the two-mode film there are various possible cases of TBD: it may happen either at single-type mode diffraction ($\beta_1 = \beta_2$) or at diffraction of modes of different types ($\beta_1 \neq \beta_2$). At $\beta_1 \neq \beta_2$ we can evaluate the mode azimuths using (12):

$$\sin\alpha_1 = \{mK_{0,y}(K_0^2 - \Delta) \pm K_{0,x}[4\beta_1^2K_0^2 - (K_0^2 - \Delta)^2]^{1/2}\}/2\beta_1K_0^2 \tag{13}$$

$$\sin\alpha_2 = \{-mK_{0,y}(K_0^2 + \Delta) \pm K_{0,x}[4\beta_2^2K_0^2 - (K_0^2 + \Delta)^2]^{1/2}\}/2\beta_2K_0^2 \tag{14}$$

where $K_{0,x}$ and $K_{0,y}$ are x- and y-components of planar K_0; $\Delta = \beta_2^2 - \beta_1^2$. To determine azimuths α_1 and α_2, we have to know the propagation constants of TE_0- and TM_0-modes. We know the value $\beta_1 = \beta_{TM_0}$ from diffraction measurements of the S_--grating, $\beta_1 = 1.5246k_0$. The $\beta_2 = \beta_{TE_0}$ value could be determined from C-grating diffraction. Direct measurements give $\beta_2 = 1.592k_0$. However, remembering that the scattering indicatrix favours the growth of C-gratings on both TE- and TM-modes, we must understand that the measured value of β_2 is an intermediate value between β_{TE_0} and β_{TM_0}. For more precise estimation we used figure 2(f). We took into account the fact that arcs 5 and 11 at $\beta_{TM_0} = 2k_x$ have the largest deviation from the incidence plane in the y-axis direction. It is the region of the vertical arc 8 of diffraction from S_--like gratings. The ratio of the distance from the intersection of arcs 5 and 8 to the distance from the intersection of arcs 11 and 8 is $d_{2y}/d_{1y} = 2 \pm 0.04$. On the other hand, this ratio is

$$\frac{d_{2y}}{d_{1y}} = \frac{n_{TE} - \sqrt{n_{TE}^2 - \sin^2\varphi}}{n_{TM} - \sqrt{n_{TE}^2 - \sin^2\varphi}}. \tag{15}$$

Calculation from (15) results in the value $\beta_2 = n_{TE}k_0 = (1.620 \pm 0.002)k_0$. We obtained a better agreement with experiment using these components in further calculations.

It is important to determine the dominant gratings (i.e. to find their $\boldsymbol{K}_0$) to explain the SAS patterns. In addition to C-gratings, there are dominant S_--like gratings creating spots 6, 9 and 7, 10 in figure 2. We refer to these SGs as secondary ones because we found that they develop only after the appearance of dominant C-gratings. Assuming that TBD is the mechanism of SG interaction, we tried to use dominant C_{TE}- and C_{TM}-gratings in the calculation of TBD. However, calculations by (13) show that obtained values of α_1 result in azimuths of modes which are not in agreement with experiment. The search for other dominant SGs has led us to the following explanation.

Waveguide modes interact with a dominant C-grating. This results in the appearance of radiative modes. One of them shows up among the others due to its intensity. It has the vector $\boldsymbol{k}_r = -k_x\boldsymbol{i}$. Its interference with the incident beam creates the so-called B-grating with $\boldsymbol{K}_B = -2k_x\boldsymbol{i}$. The appearance of B-gratings was reported earlier at small φ [24] and at large φ [25]. Since B-gratings grow in the vicinity of C-gratings, their superposition has to result in a so-called C/B-grating with vector $\boldsymbol{K}_{C/B} = \boldsymbol{K}_C + \boldsymbol{K}_B = \boldsymbol{K}_C - 2k_x\boldsymbol{i}$. There may be eight C-gratings with vectors (4) and (5), therefore eight C/B-gratings

Table 1. Comparison of measured and calculated parameters of substrate modes which create reflexes 1–7 (rows of light spots) on the sample. The numeration of reflexes is as in figure 3(a) (experiment) and figure 4(c) (theory). Value d is the distance between spots in a row; γ_d is the row's angle to the plane of incidence; k_{dx}, k_{dy} and k_d are the components and magnitude of the substrate mode.

	d (mm)	Experimental values				Calculated values			
		γ_d	k_{dx}/k_0	k_{dy}/k_0	k_d/k_0	γ_d	k_{dx}/k_0	k_{dy}/k_0	k_d/k_0
1	4.2	95.5°	−0.110	1.144	1.150	94°00′	−0.079	1.130	1.132
2	5.6	−85°	0.110	−1.263	1.267	−85°00′	0.105	−1.224	1.228
3	3.2	−71.5°	0.319	−0.954	1.006	−71°10′	0.319	−0.933	0.986
4	5.0	−66.5°	0.490	−1.128	1.229	−66°10′	0.498	−1.128	1.233
5	4.4	68°	0.445	1.101	1.188	67°30′	0.450	1.082	1.172
6	3.45	56°	0.586	0.869	1.048	59°20′	0.553	0.932	1.084
7	4.65	58°	0.635	1.016	1.198	60°20′	0.595	1.045	1.202

may exist. The vectors of the four C/B-gratings corresponding to the C-gratings from (4) are

$$\begin{aligned} \boldsymbol{K}_{\mathrm{C/B},1,2} &= -2k_x\boldsymbol{i} \pm \sqrt{\beta_{\mathrm{TM}}^2 - k_x^2}\boldsymbol{j}, \\ \boldsymbol{K}_{\mathrm{C/B},3,4} &= -2k_x\boldsymbol{i} \pm \sqrt{\beta_{\mathrm{TE}}^2 - k_x^2}\boldsymbol{j}. \end{aligned} \tag{16}$$

The vectors of the four C/B-gratings corresponding to the C-gratings from (5) are

$$\begin{aligned} \boldsymbol{K}_{\mathrm{C/B},5,6} &= -\left(\frac{\Delta}{4k_x} + 2k_x\right)\boldsymbol{i} \pm \sqrt{\beta_{\mathrm{TE}}^2 - \beta_{\mathrm{TE},x}^2}\boldsymbol{j}, \\ \boldsymbol{K}_{\mathrm{C/B},7,8} &= \left(\frac{\Delta}{4k_x} - 2k_x\right)\boldsymbol{i} \pm \sqrt{\beta_{\mathrm{TM}}^2 - \beta_{\mathrm{TM},x}^2}\boldsymbol{j}. \end{aligned} \tag{17}$$

Here $\sqrt{\beta_{\mathrm{TE}}^2 - \beta_{\mathrm{TE},x}^2} = \sqrt{\beta_{\mathrm{TM}}^2 - \beta_{\mathrm{TM},x}^2}$.

These gratings may grow immediately on scattered waveguide modes: the gratings (16) grow on TM-modes with $\beta_{1,2} = -k_x\boldsymbol{i} \pm \sqrt{\beta_{\mathrm{TM}}^2 - k_x^2}\boldsymbol{j}$ and TE-modes with $\beta_{3,4} = -k_x\boldsymbol{i} \pm \sqrt{\beta_{\mathrm{TE}}^2 - k_x^2}\boldsymbol{j}$. The gratings (17) grow on TE-modes with $\beta_{5,6} = (-\Delta/(4k_x) - k_x)\boldsymbol{i} \pm \sqrt{\beta_{\mathrm{TE}}^2 - \beta_{\mathrm{TE},x}^2}\boldsymbol{j}$ and TM-modes with $\beta_{7,8} = (\Delta/(4k_x) - k_x)\boldsymbol{i} \pm \sqrt{\beta_{\mathrm{TM}}^2 - \beta_{\mathrm{TM},x}^2}\boldsymbol{j}$.

The C/B-gratings are more regular than S$_-$-SG in spite of C/B-grating growth on ordinary Wood's anomalies. This conclusion was drawn due to the regularity of secondary gratings which are generated due to the existence of C/B-gratings (this will be shown below). The possibility of the existence of eight C/B-gratings complicates the task of calculating the secondary gratings. We have to substitute various vectors of C/B-gratings (with magnitudes $K_{\mathrm{C/B},1,2} = \sqrt{\beta_{\mathrm{TM}}^2 + 3k_x^2}$, $K_{\mathrm{C/B},3,4} = \sqrt{\beta_{\mathrm{TE}}^2 + 3k_x^2}$, $K_{\mathrm{C/B},5,6} = \sqrt{\beta_{\mathrm{TE}}^2 + 3k_x^2 + 0.5\Delta}$, $K_{\mathrm{C/B},7,8} = \sqrt{\beta_{\mathrm{TM}}^2 + 3k_x^2 - 0.5\Delta}$) into (13) and (14). We also checked the TBD of modes of the same type and different types.

There may be eight C/B-gratings with vectors (16) and (17), and on each SG there may be four cases of TBD (TBD of TE- and TE-modes, TE and TM, TM and TE, TM and TM) of which two cases (TM-mode under α_1 from (13) and TE- or TM-mode with α_2 from (14)) are not forbidden by the scattering indicatrix. Having checked all 16 cases, we compared calculated results and measurements with microphotographs of figures 3(b) and (c). It appears that the secondary grating, which creates spots 6 and 9, is on the TM-mode with $\alpha_1' = 9°10'$, which is amplified at TBD of TE- and TM-modes on the C/B-grating with $\boldsymbol{K}_{\mathrm{C/B},5}$ (see (16) and figure 4). Spots 7 and 10 correspond to the SG on the mode with $\alpha_1'' = -5°40'$, which is amplified at TBD of TM- and TM-modes on the C/B-grating with $\boldsymbol{K}_{\mathrm{C/B},8}$ (see (17) and figure 4). These SGs have calculated vectors $\boldsymbol{K}_{\mathrm{S}_{1'}} = k_0(0.743\boldsymbol{i}+0.243\boldsymbol{j})$ and $\boldsymbol{K}_{\mathrm{S}_{1''}} = k_0(0.755\boldsymbol{i} - 0.149\boldsymbol{j})$ (designations of secondary SGs are taken from [6]). The calculated values of angles of the grating vectors are $\alpha_{\mathrm{g}1}' = 18°10'$ and $\alpha_{\mathrm{g}1}'' = -11°10'$, while the measured values are $18.5° \pm 1°$ and $-12° \pm 1°$ (see figures 3(b), (c)). Good agreement of experimental and calculated values only for the case of C-gratings with $\boldsymbol{K}_5$ and $\boldsymbol{K}_8$ again confirms their dominance.

However, we must note that, though C-SGs with $\boldsymbol{K}_5$ and $\boldsymbol{K}_8$ are dominant, other C-gratings still may grow, and in figure 3(c) in the top-left corner there is a domain of S$_1$-grating with angle 22°10′ instead of 18°10′. This SG is amplified by TBD of TE- and TM-modes on the C/B-SG with $\boldsymbol{K}_{\mathrm{C/B},1}$. But such gratings are weak, and they do not create any visible reflexes.

Now let us analyse the diffraction reflexes appearing on the sample (figure 3(a)) during the process of S$_1$-grating creation. This diffraction allows us to reveal radiative modes with $k_0 < k_r < k_0 n_s$. Measurements of the intervals d between adjacent bright dots in the rays at known substrate thickness $H = 1.8$ mm allow us to define the diffraction beam's entry angles to the substrate θ_d ($\tan\theta_d = d/2H$) and the tangential component of the substrate mode ($k_d = k_0 n_s \sin\theta_d$). Having measured angles $\gamma_d = \angle(\boldsymbol{k}_d, \boldsymbol{k}_x)$, we calculate components k_{dx} and k_{dy} of substrate modes (see table 1).

First let us consider reflexes 1 and 2 appearing simultaneously with S$_1$-gratings. They are explained by diffraction of modes of C-gratings on S$_1'$- or S$_1''$-grating. Reflex 1 is created by diffraction of the mode of the C-grating with $\boldsymbol{K}_5$ on S$_1''$-SG, and reflex 2 is created by the mode of the C-grating with $\boldsymbol{K}_8$ diffracted on the S$_1'$-grating at $m = -1$ (see table 1). Two remaining variants of such a diffraction create not substrate modes but waveguide ones.

Reflexes 3–5 in figure 3 appear after large exposition and have a somewhat different origin. They appear as a result of diffraction of the laser beam on some gratings which do not produce diffraction into air. Analysis based on found values of k_{dx} and k_{dy} shows that these new reflexes are due to diffraction in -1 order on TM-gratings. We made the following assumption explaining reflexes 3–5 and associate

this assumption with the appearance of regular secondary S_1'- and S_1''-gratings. Propagating in the film, dominant TM-modes, excited on S_1'- and S_1''-gratings, may interact with weaker SGs. The existence of these S$_-$-like gratings is confirmed by the existence of their diffraction reflexes (figure 2(e), arc 8). A TBD of mode β_1 of the S_1'-SG or S_1''-SG on these weak gratings is possible. Each known mode β_1 may take part in two cases of TBD on TM-gratings, thus amplifying two TM-modes. So there is strong feedback in the growth of two SGs. At the existence of two strong TM-modes (S_1'- and S_1''-modes) there are four weak SGs which are amplified. These SGs are tertiary, because they intensively grow only after the appearance of dominant secondary SGs. When the laser beam diffracts on four tertiary SGs, it creates four radiative modes. Three of them create reflexes 3, 4 and 5 in figure 3, while the fourth one leaves the film at a sliding angle because its tangential component is less than k_0. Reflexes 3 and 5 are due to TBD with S_1''-mode, while reflex 4 is due to TBD with S_1'-mode. The calculated values are in agreement with experiment even better than for secondary gratings (see table 1). This is explained by the fact that at TBD creating tertiary SGs there are TM-SG and two TM-modes. It is known that the effective refractive index of TM-modes has a steady value (while the TE-index changes at initial stages of irradiation), and we better control its value by diffraction arcs appearing on the screen during irradiation.

The weaker dot-like reflexes 6 and 7 (figure 3) are created in a third way. One can see on the substrate the weak light lines, which pass through reflexes 5 and 6. These lines correspond to the many substrate modes which are created at diffraction of TM-modes of S$_-$-like SGs on the S_1'-grating at $m = -1$. So S$_-$-like SGs synchronously create arc 8 on the screen (see figure 2) and lines on the sample. The absence of such lines in the lower half of the sample (they should appear at analogous diffraction on S_1''-SG) is explained by scattering indicatrices at $\chi = 15°$ (see (8)): the corresponding TM-SGs are too weak to produce visible spots. Understandably, reflexes 5 and 6 are created by TM-mode diffraction because they are the bright parts of the weak TM-lines. But row 7 has a larger distance between spots and appears to be created by a TE-mode diffracted on the same S_1'-SG. The existence of a strong TM-mode of reflex 6, and especially the existence of the TE-mode of reflex 7 (which is in contradiction with the scattering indicatrix), at first glance is puzzling. But we found that TBD on dominant gratings explains these reflexes too. Above we considered TBD on C/B-gratings (it creates S_1'- and S_1''-SGs), and TBD of modes of S_1'- and S_1''-SGs (creates tertiary SGs 3, 4 and 5). Now consider TBD on the last pair of the three pairs of dominant (primary and secondary) gratings: TBD on C-gratings.

Calculations by (13) and (14) were analogous to previous cases (except for the fact that the C-gratings are antiparallel, and we can consider TBD on only one of them). Actually, there may be four pairs of C-gratings, and four cases of TBD on each pair. But among these 16 cases only six may create such waveguide modes that produce substrate modes through diffraction on S_1'- or S_1''-SG, and four of these cases are forbidden by the scattering indicatrix. The two remaining variants are the reflexes 6 and 7. They are created due to the existence of, correspondingly, TM- and TE-modes taking part in TBD on the C-grating with $\boldsymbol{K}_5$ or $\boldsymbol{K}_8$ at TM–TM and TE–TM cases of TBD (see table 1). These TM- and TE-modes diffract on S_1''-SG and form reflexes 6 and 7.

So, considering various cases of TBD involving all six dominant SGs (primary and secondary), we obtain a complete explanation of all the reflexes on the screen and sample. Therefore the importance of considering the TBD at SG development is proved.

The results of experiments and calculations are presented also with the Ewald's polar diagrams plotted in the (k_x, k_y) plane (figure 4). The circles with radii β_{TE} and β_{TM} are plotted in the diagrams. The inner circle has radius $k_0 = 2\pi/\lambda$. In figure 4(b) there are vectors of primary regular C- and C/B-gratings and vectors of secondary regular S_1-gratings on TM-modes. All the grating vectors are plotted from the point $A(k_x, 0)$. Also in figure 4(b) in the central part there are geometrical places (arcs) of the ends of leaky mode vectors k_{d} and k_{r} appearing correspondingly at beam diffraction and mode diffraction on gratings; see (2) and (11). Vectors of leaky modes are plotted from point O. These arcs are seen on the screen because $k_{\mathrm{r}}, k_{\mathrm{d}} < k_0$ (see figure 2). The points on the vertical arc are the diffraction reflexes ($m = -1$) from regular S_1'- and S_1''-gratings (see spots 6 and 7 in figure 2(c)–(f)). The vertical arc passing across them (corresponds to arc 8 in figure 2) is the many diffraction reflexes from S$_-$-like gratings. The horizontal arc passing across point B (it is arc 5 in figure 2), $\mathrm{OB} = -k_x$, is the result of diffraction of TE-modes with maximum intensities on the dominant C-grating with $\boldsymbol{K}_8$.

The polar diagram in figure 4(c) demonstrates tangential components of leaky modes observed on the substrate, and vectors of the tertiary gratings found. Solid lines correspond to experiment; dashed lines show the results of calculations (see table 1). Vectors 3, 4, 5 (plotted from the point O) correspond to observed leaky modes ($m = -1$) arising at beam diffraction on TM-gratings with vectors 3, 4, 5 (grating vectors are plotted from point A). One can see that the experimental and calculated results are close; for example, for reflexes 2–5 they have almost merged (see figure 4(c)).

6. Conclusion

The appearance of spontaneous gratings must be taken into account at the creation of holograms and holographic gratings in films of various light-sensitive materials, because they create additional noise. Unlike holographic gratings, spontaneous gratings need only one inducing beam to appear, and they are investigated at single laser beam action.

We found that under conditions of strong competition of scattered TE_0- and TM_0-modes, spontaneous grating formation in light-sensitive AgCl–Ag films substantially depends on the linear polarization azimuth of the inducing laser beam. While at P-polarization spontaneous gratings grow on scattered TM_0-modes (S$_-$-like gratings), a comparatively small deviation of the polarization plane from the plane of incidence results in a completely new scenario of spontaneous grating development. A quasi-continuous spatial spectrum of S$_-$-like gratings on β_{TM_0}-modes at $\chi = 0°$ is replaced by regular S_1'- and S_1''-gratings. Their appearance at mixed S/P-polarization is associated with the development of regular

primary C- and C/B-gratings on both TE_0- and TM_0-modes. We found that the two-dimensional Bragg diffraction of TE_0- and TM_0-modes on dominant C/B-gratings is the main reason for regular TM_0-grating appearance. This process is favoured by azimuthal distribution of scattered radiation at $\chi \neq 0$. In their turn, intensive enough TM_0-modes (excited on S_1'- and S_1''-gratings) promote the appearance of new tertiary regular gratings found by us due to diffraction into the substrate.

So two-dimensional diffraction appears to be a very important mechanism of spontaneous grating interaction in their development, because it may be used to either amplify or suppress a chosen type of spontaneous grating by varying the irradiation conditions. Besides, the existence of this interaction mechanism reduces the role of the scattering indicatrix, and this may allow us to model the development of spontaneous gratings mathematically without considering fluctuations of the scattering indicatrix.

References

[1] Chumash V, Cojocary I, Fazlo E, Michelotti F and Bertolotti M 1996 Nonlinear propagation of strong laser pulses in chalcogenide glass films *Progress in Optics* vol 36, ed E Wolf (Amsterdam: Elsevier) pp 1–45

[2] Dyer P E and Farley R J 1993 *J. Appl. Phys.* **74** 1442–4

[3] Andrews J H and Singer K D 1993 *Appl. Opt.* **32** 6703–9

[4] Hariharan P 1996 *Optical Holography. Principles, Techniques and Applications* (Cambridge: Cambridge University Press)

[5] Fournier J-M 2004 *Holography. The First 50 Years* (*Springer Series in Optical Sciences* vol 78) (Berlin: Springer)

[6] Ageev L A and Miloslavsky V K 1995 *Opt. Eng.* **34** 960–72

[7] Ageev L A, Miloslavsky V K and Lymar V I 1990 *Opt. Spektrosk.* **69** 415–20 (in Russian)

[8] Siegman A E and Fauchet P M 1986 *IEEE J. Quantum Electron.* **22** 1384–403

[9] Bonch-Bruevich A M, Libenson M N, Makin V S and Trubaev V V 1992 *Opt. Eng.* **31** 718–30

[10] Lymar V I, Miloslavsky V K and Ageev L A 1993 *Opt. Spektrosk.* **74** 183–8 (in Russian)
Lymar V I, Miloslavsky V K and Ageev L A 1993 *Opt. Spectrosc.* **74** 183–8 (Engl. Transl.)

[11] Miloslavsky V K, Bondarenko O V and Ageev L A 2003 *Opt. Commun.* **228** 365–72

[12] Miloslavsky V K, Makovetsky E D and Ageev L A 2003 *Opt. Commun.* **232** 303–12

[13] Ageev L A, Miloslavsky V K and Varminsky M V 1997 *Opt. Spektrosk.* **83** 159–64 (in Russian)
Ageev L A, Miloslavsky V K and Varminsky M V 1997 *Opt. Spectrosc.* **83** 159–64 (Engl. Transl.)

[14] Young J F, Preston J S, van Driel H M and Sipe J E 1983 *Phys. Rev.* B **27** 1155–72

[15] Arutyunyan R V, Baranov V Yu, Bolshov L A, Malyuta D D and Sebrant A Yu 1989 *Laser Beam Effects on Materials* (Moscow: Nauka) (in Russian)

[16] Bohren C F and Huffman D R 1983 *Absorption and Scattering of Light by Small Particles* (New York: Wiley)

[17] Adams M J 1981 *An Introduction to Optical Waveguides* (New York: Wiley)

[18] Yariv A and Yeh P 1984 *Optical Wave in Crystals* (New York: Wiley)

[19] Blokha V B, Ageev L A and Miloslavsky V K 1985 *Zh. Tekhn. Fiz.* **55** 1967–72 (in Russian)

[20] Ageev L A, Miloslavsky V K and Nahal A 1998 *Pure Appl. Opt.* **7** L1–5

[21] Ageev L A, Miloslavsky V K and Larionova E I 2000 *Opt. Spektrosk.* **89** 1032–39 (in Russian)
Ageev L A, Miloslavsky V K and Larionova E I 2000 *Opt. Spectrosc.* **89** 1032–39 (Engl. Transl.)

[22] Marcuse D 1972 *Light Transmission in Optics* (New York: Van Nostrand-Reinhold)

[23] Semenov A S, Smirnov V L and Shmalko A V 1990 *The Integrated Optics for Systems of Transmission and Treatment of Information* (Moscow: Radio i Svyaz) (in Russian)

[24] Miloslavsky V K, Nahal A and Ageev L A 1999 *Opt. Commun.* **164** 269–76

[25] Miloslavsky V K, Ageev L A and Lymar V I 1990 *Proc. SPIE* **1440** 90–7